PAPER

Check for updates

Influence of structure phase transition on the thermoelectric properties of $Cu_2Se_{1-x}Te_x$ liquid-like compounds

Trung Kien Mac, [ab] Thi Thu Ta, [ab] Huu Tuan Nguyen, [ID] [bc] Van Du Nguyen, [a] Thi Lan Huong Pham, [d] Van Thiet Duong, [e] Tran Dang Thanh, [ef] Bach Thang Phan [ID] [g] and Anh Tuan Duong [ID] *[ab]

Copper chalcogenide $Cu_2(Se,Te)$ compounds are well known as typical p-type thermoelectric materials with a figure of merit (ZT) that can be optimized by the ratio of Se : Te. Here, by using the mechanical alloying and solid-state reaction methods, Te was substituted into Se sites within Cu_2Se as the formula $Cu_2Se_{1-x}Te_x$ ($x = 0.1, 0.2, 0.25,$ and 0.3). The observed changes in structural phase, grain morphologies, and grain size were recorded by XRD and FE-SEM imaging with the appearance of the secondary phase of Cu_2Te, with a Te content of $x = 0.25$. The layered structure morphology was observed more clearly at the high Te content. The electrical conductivity was greatly increased with enriched Te content while the maximum Seebeck coefficient was obtained in the $Cu_2Se_{0.75}Te_{0.25}$ sample. Accordingly, a power factor value of up to 9.84 µW cm^{-1} K^{-2} at 773 K was achieved. The appearance of a Cu_2Te phase with a Te content of 0.25 created a structural phase transition which results in a ZT value of 1.35 at 773 K in the $Cu_2Se_{0.75}Te_{0.25}$ sample.

1. Introduction

Thermoelectric (TE) materials are of increasing interest because they can directly convert waste heat from furnaces, vehicle engines, factories, or human bodies to electric power without moving parts.[1] The performance of TE materials is determined by the figure of merit (ZT), defined as $ZT = S^2\sigma T/\kappa$, where S is the Seebeck coefficient, σ is the electrical conductivity, T is the absolute temperature, and κ is the total thermal conductivity ($\kappa = \kappa_E + \kappa_L$, where κ_E and κ_L are the electronic and lattice contributions, respectively).[2] To maximize the ZT value of materials, larger power factor ($S^2\sigma$) and lower thermal conductivity (κ) of materials are required.[3] The Seebeck coefficient can

be improved by some methods such as resonance doping,[4,5] band convergence,[6] hyperconvergence,[7,8] Rashba splitting,[9] band gap enlargement,[10,11] and breaking of crystal mirror symmetry.[12] The balance between low effective mass and high mobility of charge carriers can enhance their electrical conductivity.[3,13] The thermal conductivity can be minimized by adding a number of interfaces and phonon scattering centers.[14]

Copper-base composites have been well-known as a high ZT value material. The copper chalcogenide compounds such as the Cu-base diamond-like compound (Cu_2SnSe_3, Cu_2GeSe_3, Cu_3SbSe_3, $CuSbSe_2$, $CuGaTe_2$ or $CuInTe_2$,...) or Cu-base liquid-like compound $Cu_2(S, Se, Te)$ have high ZT value due to high electrical conductivity and low lattice thermal conductivity while other Cu-base such as the CuI compounds or CuI-based coordination polymer precursors exhibited high Seebeck coefficient.[15–19] Among of the copper chalcogenide compounds, copper selenide (Cu_2Se) has well-known as an excellent thermoelectric material due to its high ZT value, low cost, nontoxic, and tunable electrical transport properties. Belong to the group of liquid-like compounds, Cu_2Se has a complex crystal structure with two main structural phases – α phase below 414 K and β phase formed above 414 K.[20] In the high-temperature phase of Cu_2Se, copper (Cu) ions are random located (liquid-like ions) inside the rigid sublattice of Se, leading to weak bonding and enhancing lattice phonon scatter.[16,21] Until now, to increase the ZT value of Cu_2Se, most researchers have focused on the control of doping elements and contents to modify electrical transport properties; nano-structuring to reduce thermal conductivity,

[a]Faculty of Materials Science and Engineering, Phenikaa University, Yen Nghia, Ha-Dong District, Hanoi, 12116, Vietnam. E-mail: tuan.duonganh@phenikaa-uni.edu.vn

[b]Phenikaa Research and Technology Institute (PRATI), A&A Green Phoenix Group, 167 Hoang Ngan, Hanoi, 10000, Vietnam

[c]Faculty of Electrical and Electronic Engineering, Phenikaa University, Hanoi, 12116, Vietnam

[d]Faculty of Biotechnology, Chemistry and Environmental Engineering, Phenikaa University, Hanoi, 10000, Vietnam

[e]Graduate University of Science and Technology, Vietnam Academy of Science and Technology, 18-Hoang Quoc Viet, Cau Giay, Hanoi, 10000, Vietnam

[f]Institute of Materials Science, Vietnam Academy of Science and Technology, 18-Hoang Quoc Viet, Cau Giay, Hanoi, 10000, Vietnam

[g]Center for Innovative Materials and Architectures, Vietnam National University, Ho Chi Minh City, Vietnam

and optimizing the growth method to control the structure and defect of materials for maximizing ZT value. Through the optimization of fabrication methods such as the hydrothermal, high-energy ball milling technique combined with spark plasma sintering (SPS), hot-pressing; and the control of the fabrication parameters (temperature and pressure), the ZT values of pure Cu_2Se can achieve from 1.0 to 1.8 at around of 800–900 K.[22–27] Fabrication of Cu_2Se nanostructure leads to the formation of scattered interfaces, thus to reduce lattice thermal conductivity. On the other hand, under the nanoscale, quantum confinement effects enhance the electron density of states near the Fermi level, leading to the improvement of the Seebeck coefficient.[16] The ZT values of Cu_2Se nanostructure can be achieved above 2.0. For the doping method, the best TE performance with a ZT value of 2.62 was obtained at 756 °C for the bulk $Cu_{1.94}Al_{0.02}Se$.[28] The good TE performance achieved by wet chemical method with the ZT from 0.9 to 1.6.[29,30] Although the above manufacturing methods have resulted in well-improved TE properties of materials, they also have several limitations, which require expensive equipment and complex manufacturing protocol. Especially, for the melting process, which is necessary to rise to an extremely high temperature, takes more time, and the wet chemical method only produces a small amount of sample.

In the liquid-like compound of Cu_2(S, Se, Te) group, the modification of S, Se, and Te elements content to maximize ZT value is attracting many research groups. Especially for control of Te contents in Cu_2(Se, Te) material systems. In 2016, S. Butt *et al.* controlled Te doping contents (as Te-5%, Te-10%, Te-15%, and Te-20%, respectively in Cu_2Se) and Te-10% doping in Cu_2Se achieved the highest ZT value of 1.9 at 873 K.[31] At lower 10% of Te doped Cu_2Se, L. Yang *et al.* reported that the highest ZT value of 1.76 was observed at 850 K for $Cu_2Se_{0.98}Te_{0.02}$ sample while Y. B. Zhu *et al.* described the same composition of $Cu_2Se_{0.98}Te_{0.02}$ but using a different growth method, the ZT value could be achieved up to 1.25 at 773 K.[20,32] K. Zhao *et al.* studied the thermoelectric properties of the series $Cu_2Se_{1-x}Te_x$ ($x = 0.2, 0.3, 0.5$, and 0.7). The result showed that the crystal structure of the sample with Te content of 0.2 ($Cu_2Se_{0.8}Te_{0.2}$) was nearly the same as Cu_2Se, indicating no structural change.[33] They also reported that the highest ZT value of 1.4 could be achieved for $Cu_2Se_{0.7}Te_{0.3}$ at 1000 K with the Cu_2Te phase observed. By using the chemical method, F.-H. Lin *et al.* reported the ZT value of 1.2 at 773 K and 1.4 at 920 K for the $Cu_2Se_{0.96}Te_{0.04}$ sample.[34] At around the transitional phase of the $Cu_2Se_{1-x}Te_x$ (with Te contents between 0.2 to 0.3), the influence of Te content on the thermoelectric properties of these materials should be clarified.

Here, we focus on the $Cu_2Se_{1-x}Te_x$ composition with Te contents of 0.1, 0.2, 0.25, and 0.3 by using a simple method, mechanical alloying combined with solid-state reaction (pressing and sintering). We found that, at 0.25 of Te content, the Cu_2Te phase appeared, and a structural phase transition was observed. Especially, a new structural morphology was observed by FE-SEM images in the composition of $Cu_2Se_{0.75}Te_{0.25}$ and $Cu_2Se_{0.7}Te_{0.3}$. The highest ZT value of 1.35 was achieved at 773 K for the $Cu_2Se_{0.75}Te_{0.25}$ sample.

2. Experimental

High purity powder of Cu (99.99%), Se (99.99%), and Te (99.99%) were weighed, according to the chemical compositions of $Cu_2Se_{1-x}Te_x$ ($x = 0.1, 0.2, 0.25$, and 0.3). The stoichiometric elements were loaded into a tungsten carbide jar with tungsten carbide balls for mechanical alloying (MA) by a high-energy ball mill (FRITSCH Pulverisette 7, Germany) for 10 hours with the speed of 700 rpm. The nano-powder was loaded into a Ø 12 mm diameter mold and pressed under uniaxial pressure of 50 MPa at 523 K for 1 hour. The obtained samples were sintered at 873 K for 1 hour in an argon atmosphere. The crystal structure was investigated by X-ray diffraction (XRD) by using XRD EQUINOX 5000 Thermo Scientific, France with Cu-Kα radiation, $\lambda = 1.54056$ Å. Field-Emission Scanning Electron Microscopy (FE-SEM) was used to obtain the crystal morphologies. The electrical conductivity σ and Seebeck coefficient S were measured by a thermoelectric measurement system (Linseis-LSR3, Germany) using a four-probe contact method in a Helium atmosphere and a temperature range of 300 K to 773 K. The total thermal conductivity (κ) was calculated by the formula $\kappa = DC_pd$. The thermal diffusivity (D) and the specific heat capacity (C_p) of all bulk samples were measured by NETZSCH LFA 467 using the laser flash method in the Ar atmosphere. The sample densities (d) were obtained by the basic calculation $d = mV^{-1}$, where m is the mass of the sample and V is its volume.

3. Results and discussion

The crystal structure of bulk $Cu_2Se_{1-x}Te_x$ ($x = 0.1, 0.2, 0.25$, and 0.3) was observed by XRD patterns as shown in Fig. 1, corresponding to with two standard identification patterns of α-Cu_2Se (card #96-155-6748) and Cu_2Te (card #96-152-6238). At low Te content samples ($Cu_2Se_{0.9}Te_{0.1}$ and $Cu_2Se_{0.8}Te_{0.2}$), the XRD patterns were well-matched with trigonal α-Cu_2Se (space group $R\bar{3}m$). However, the XRD peaks shifted to a lower 2θ value with an increase of Te content, indicating that Te atoms substituted to Se sites in the Cu_2Se lattice. A structural transformation of $Cu_2Se_{1-x}Te_x$ was clearly observed at the proposed samples with the higher Te contents of $x = 0.25$ and 0.3. Particularly, the α-Cu_2Se (107) diffraction peak at 2θ around 40° disappeared, meanwhile, a secondary phase of Cu_2Te appeared (the Cu_2Te peaks were marked (*) in XRD patterns), suggesting the formation of Cu_2Se/Cu_2Te hybrid structure at a Te content of 0.25. The structural phase transition of $Cu_2Se_{1-x}Te_x$ was also observed by K. Zhao *et al.* with $x \geq 0.3$.[33] The enlarged patterns in the 2θ range of 34–40.5° were highlighted in Fig. 1b. The left shift of XRD peaks with increasing Te content indicated an expansion of lattice parameters.

Fig. 2 demonstrates the increasing of a and c lattice parameters from 4.08 Å to 4.16 Å and 19.86 Å to 20.07 Å, respectively with Te content from $x = 0$ to $x = 0.3$. It can be explained by the substitution of the larger ionic radius of Te (0.221 nm) than that of Se (0.198 nm). The tellurium concentration gradually increased, and Te elements replaced the Se position until the saturation state was reached ($x = 0.25$). The leftover Te formed
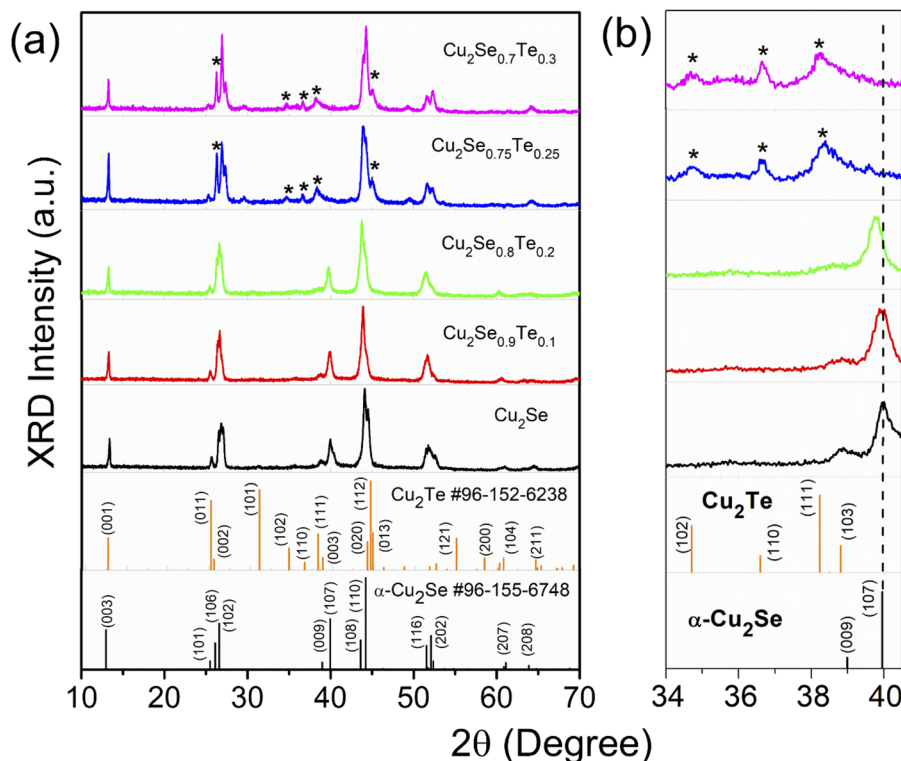
Fig. 1 The room temperature X-ray diffraction of (a) $Cu_2Se_{1-x}Te_x$ ($x = 0$; 0.1; 0.2; 0.25; and 0.3) and standard cards of α-Cu_2Se and Cu_2Te; (b) larger view of 2θ range from 34 to 40.5°.
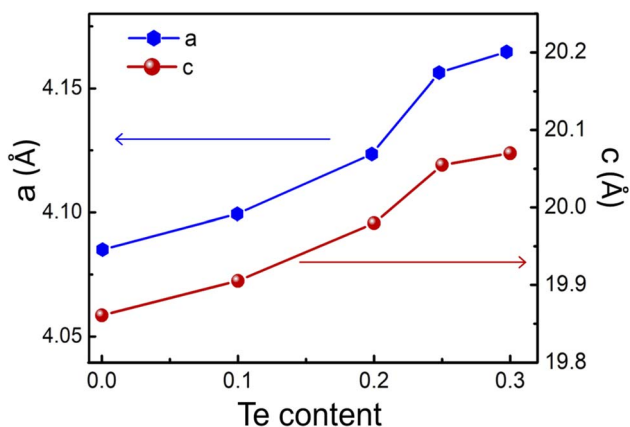

Fig. 2 The increase of "a" and "c" lattice parameters with the increasing Te content.

in the Cu_2Te phase, which leaded to a change in the XRD patterns and the morphological structure (discuss later) of the proposed samples.

Surface morphology of $Cu_2Se_{1-x}Te_x$ ($x = 0.1$, 0.2, 0.25, and 0.3) was observed by Field-emission scanning electron microscopy (FE-SEM) as shown in Fig. 3. The typical layer structure of samples was remarkably formed with the increasing Te doping content. Especially in samples with higher Te content ($x = 0.25$ and 0.3), the grain morphologies and grain boundaries markedly changed. The average grain size of $Cu_2Se_{0.75}Te_{0.25}$ and

$Cu_2Se_{0.7}Te_{0.3}$ was around 2.5 μm and 3.4 μm, respectively. A lamellar microstructure with an average thickness of a few nm was clearly observed in the high content of Te samples. The change of morphology and structure induces the improvement of electrical conductivity, which was discussed below.

The temperature dependence of electrical conductivity (σ) of $Cu_2Se_{1-x}Te_x$ ($x = 0.1$, 0.2, 0.25, and 0.3) was shown in Fig. 4a. The electrical conductivity of all samples decreased with higher temperature, indicating that all samples showed a degenerate semiconductor. An anomalous point at around ~400 K of electrical conductivity data is attributed due to the phase transition from α-phase to β-phase of Cu_2Se.[35,36] The σ value of all samples as a function of temperature above 400 K was decreased, indicating a typical degenerate semiconducting behavior. Thus, with an increasing measuring temperature, there are fewer charge carriers generated while the contribution of the decrease in carrier mobility is large, leading to a decrease in electrical conductivity. Besides, the electrical conductivity greatly increases with the increasing Te content. It can be explained by the higher intrinsic electrical conductivity of Cu_2Te is greatly higher than that of Cu_2Se.[16,20,33,37,38] The highest value of electrical conductivity was observed in the $Cu_2Se_{0.75}$-$Te_{0.25}$. It is around 54% higher than that of $Cu_2Se_{0.09}Te_{0.0.1}$ in the temperature range from 300 K to 773 K. The light-decreasing electrical conductivity of the $Cu_2Se_{0.7}Te_{0.3}$ sample could be explained by the reduction of Cu^{2+} ions due to the Cu_2Te phase formation. K. Zhao *et al.* also observed a decreasing in the

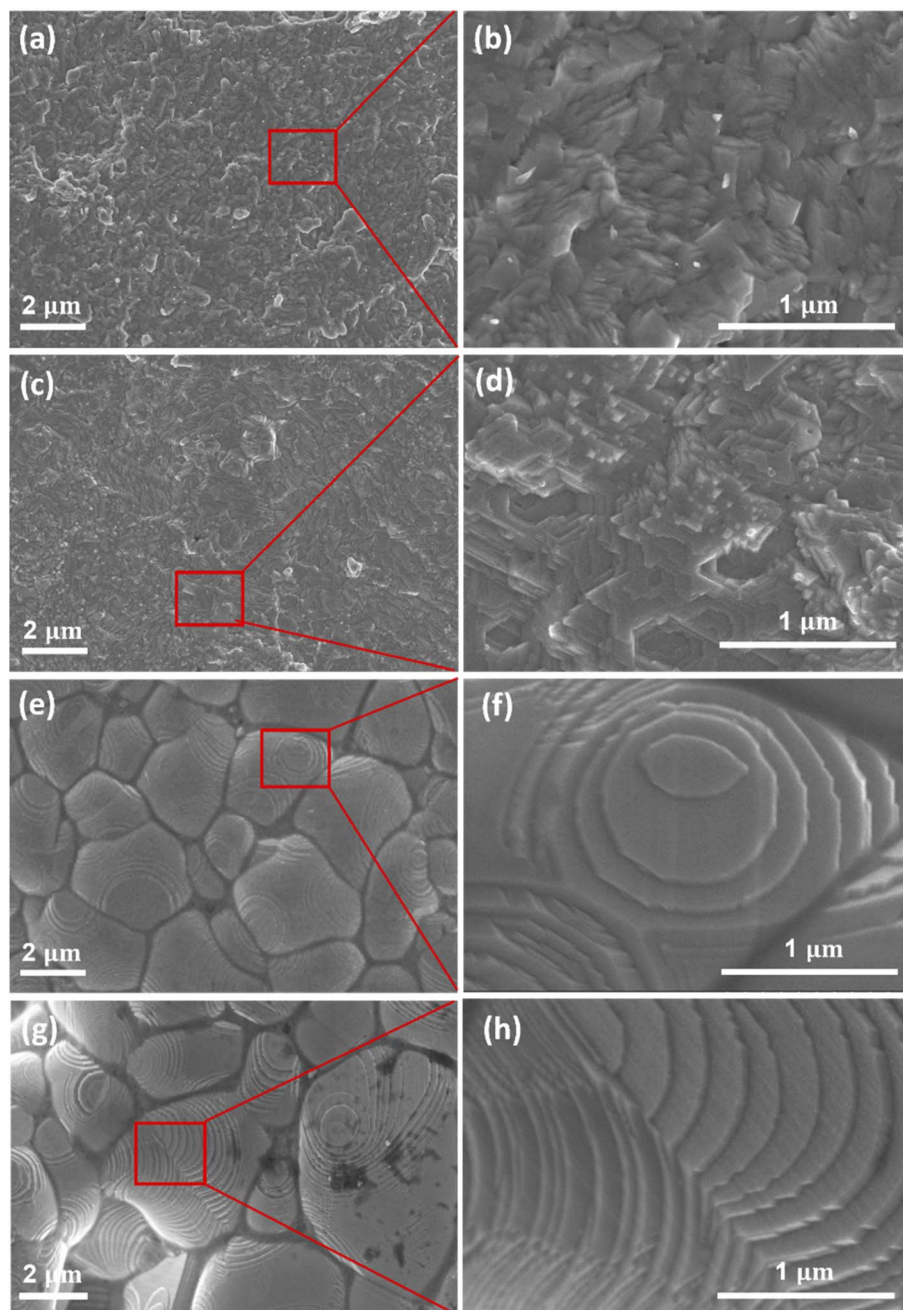Fig. 3 FE-SEM images show the morphologies of $Cu_2Se_{1-x}Te_x$ (a) $x = 0.1$; (c) $x = 0.2$; (e) $x = 0.25$; (g) $x = 0.3$; (b), (d), (f) and (h) are higher magnification of the red square in (a), (c), (e) and (g), respectively.

carrier concentration of $Cu_2Se_{0.7}Te_{0.3}$, compared to other doping samples.[33]

Seebeck coefficient as a function of temperature for all samples was presented in Fig. 4b. The positive Seebeck coefficient sign of all samples indicates that dominant charge carriers were holes and all samples showed p-type semiconducting behavior. As a type of degenerate semiconductor, the Seebeck coefficient of samples increased with an increase in temperature due to the electron–phonon scattering. In the temperature range from 300 K to 773 K, the maximum Seebeck coefficient of 135 $\mu V\ K^{-1}$ was achieved in $Cu_2Se_{0.75}Te_{0.25}$ sample, which can

be related to the local thermal gradient due to the difference in the thermal conductivity of Cu_2Te and Cu_2Se.

The thermoelectric power factor was calculated by $S^2\sigma$ as shown in Fig. 5a. The electrical conductivity increased with increasing Te content while the Seebeck coefficient was still high, resulting in the highest power factor of 9.84 $\mu W\ cm^{-1}\ K^{-2}$ at 773 K in $Cu_2Se_{0.75}Te_{0.25}$ sample. The non-linear PF at around 400 K was due to the phase transition from α-phase to β-phase of Cu_2Se.

The temperature-dependent total thermal conductivity (κ) of $Cu_2Se_{1-x}Te_x$ samples was presented in Fig. 5b. Those Te-doped

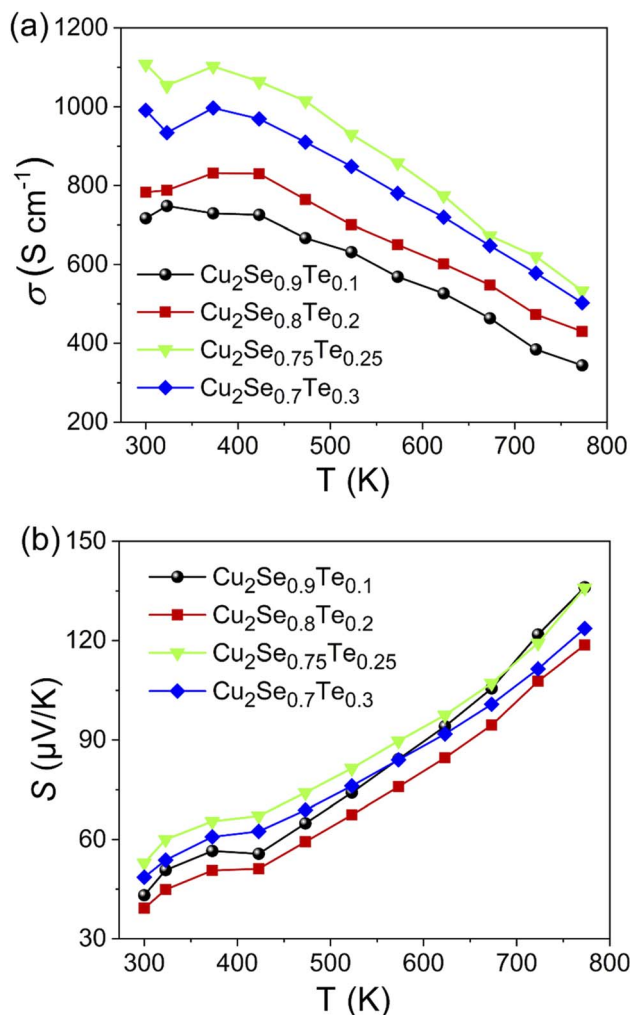Fig. 4 Temperature-dependent electronic transport properties of $Cu_2Se_{1-x}Te_x$ ($x = 0.1$; 0.2; 0.25; 0.3). (a) Electrical conductivity (σ), (b) Seebeck coefficient (S).
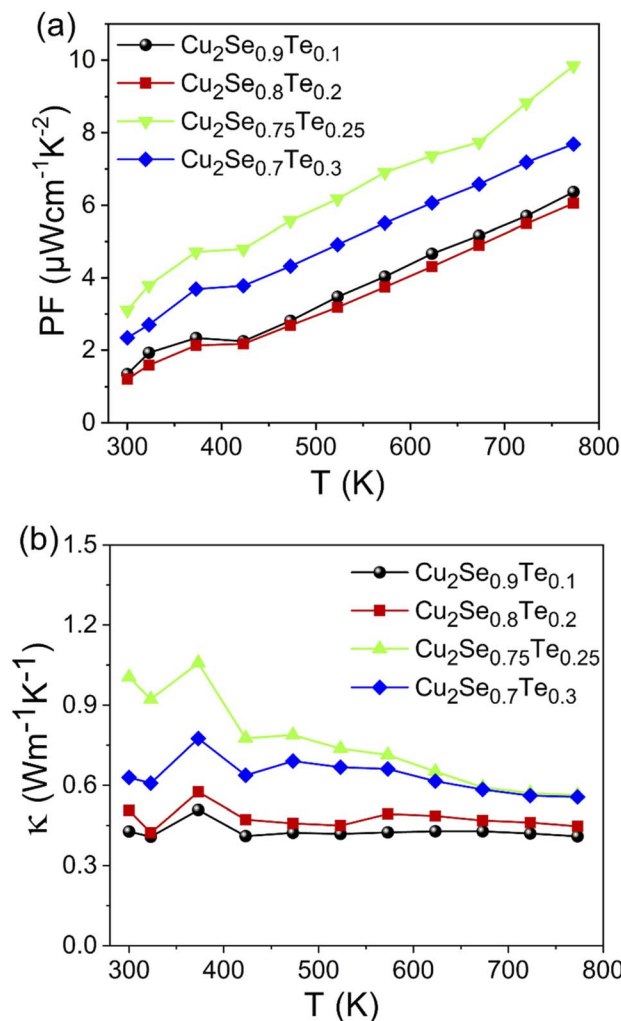

Fig. 5 The temperature dependent (a) power factor and (b) thermal conductivity of $Cu_2Se_{1-x}Te_x$ ($x = 0.1$; 0.2; 0.25; 0.3).

Cu_2Se samples also possessed very low total thermal conductivity, according to what we initially envisioned based on their natural liquid-like structures. As a general thermoelectric semiconductor, κ_L decreases due to the enhanced phonon scattering. Furthermore, combined with the trend of the electrical conductivity, it could be concluded that the carrier thermal conductivity did not have much change. Thus, as the measuring temperature increased, the total thermal conductivity decreased, except for the anomalous point near 400 K, where the phase transition (Cu_2Se) occurred. Additionally, above 400 K, the thermal conductivity of $Cu_2Se_{0.75}Te_{0.25}$ and $Cu_2Se_{0.7}Te_{0.3}$ samples decreased while it was almost maintained in the samples with low Te ($x = 0.1$ and 0.2) with increase in measuring temperature. This phenomenon could be explained *via* the decrease of the lattice thermal conductivity at the synthetic samples with high amount of Te-doped. In contrast, the slight decrease in thermal conductivity at the lower Te-doped samples was due to the balance between κ_E and κ_L. Further, the increase in thermal conductivity with increasing Te

content also indicates that the phase transition arising from the formation of the Cu_2Te phase contributed to the increasing thermal conductivity. It needs to be stressed that the thermal conductivity of Cu_2Te was higher than that of Cu_2Se. So, the formation of Cu_2Te in samples impacted to the increasing thermal conductivity.

The temperature dependence thermoelectric figure of merit (ZT) of $Cu_2Se_{1-x}Te_x$ ($x = 0.1$, 0.2, 0.25, and 0.3) was shown in Fig. 6a. The ZT values of all samples were increased with increasing temperature. With the balance of σ, S, and κ values, the highest ZT of ~1.35 was obtained at $Cu_2Se_{0.75}Te_{0.25}$, which owned the great power factor (9.84 $\mu W\ cm^{-1}\ K^{-2}$ at 773 K) and ultra-low thermal conductivity (0.56 $W\ m^{-1}\ K^{-2}$ at 773 K). At below 800 K, the ZT value in this work is almost higher than those of the pristine p-type Te-doped copper selenide materials in some previous reports under the different Te doping contents and synthetic method (Fig. 6b).[20,31–34,39,40] In the Te contents range from $x = 0.2$ to 0.3, we found that the transition phase point at Te of 0.25 achieved the highest ZT value, compared with other Te contents. K. Zhao *et al.* investigated the thermoelectric
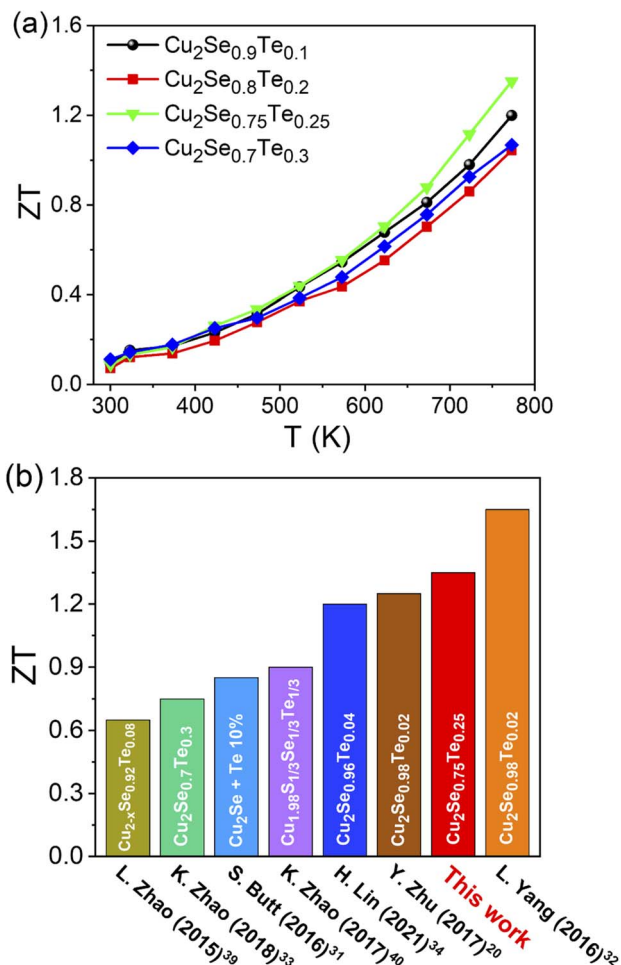
Fig. 6 (a) The thermoelectric figure of merit (ZT) of $Cu_2Se_{1-x}Te_x$ (x = 0.1; 0.2; 0.25; 0.3) and (b) comparison of ZT (T = 773 K) for present work with that reported in typical literatures of Te-doped copper selenide materials.

properties of $Cu_2Se_{1-x}Te_x$ (x = 0 to 1) solid solutions and they found the highest ZT value with x = 0.3 but the series of samples of x = 0.25 was missed.[33]

4. Conclusions

In summary, the $Cu_2Se_{1-x}Te_x$ (x = 0.1, 0.2, 0.25, and 0.3) compounds have been successfully prepared by mechanical alloying combined with a solid-state reaction method. The structural phase transition of $Cu_2Se_{1-x}Te_x$ was observed at Te content of 0.25 which obtained the highest ZT value of 1.35. A phase transition at 400 K from the $\alpha \rightarrow \beta$ of all samples has been observed and confirmed using the measured results of electrical and thermal properties. Via the XRD and FE-SEM results, the change in crystal structure and morphology was observed according to Te content. By a more simple synthetic method, the obtained ZT value in this study has higher than that of almost previous study results. More interestingly, the optimization of fabrication parameters of $Cu_2Se_{0.75}Te_{0.25}$ can lead to enhancing the ZT value of this material.

Author contributions

T. K. Mac, and T. T. Ta, synthesized the $Cu_2Se_{1-x}Te_x$ samples and performed the electrical conductivity and Seebeck coefficient experiments. V. D. Nguyen measured thermal conductivity, H. T. Nguyen, V. T. Duong, and T. L. H. Pham edited the manuscript and performed FE-SEM experiments. T. D. Thanh performed XRD experiments and edited the manuscript. B. T. Phan edited the manuscript. T. K. Mac wrote the paper with discussion and comments from all the authors. A. T. Duong supervised the project.

Conflicts of interest

There are no conflicts to declare.

Acknowledgements

References

1 M. Hamid Elsheikh, D. A. Shnawah, M. F. M. Sabri, S. B. M. Said, M. Haji Hassan, M. B. Ali Bashir and M. Mohamad, *Renewable Sustainable Energy Rev.*, 2014, **30**, 337–355.

2 D. Rowe and C. Bhandari, *CRC Handbook of Thermoelectrics*, CRC Press, 2018.

3 G. J. Snyder and E. S. Toberer, *Nat. Mater.*, 2008, **7**, 105–114.

4 U. S. Shenoy, K. D. Goutham and D. K. Bhat, *J. Alloys Compd.*, 2022, **921**, 165965.

5 D. K. Bhat and U. S. Shenoy, *Mater. Today Phys.*, 2019, **11**, 100158.

6 U. S. Shenoy, K. D. Goutham and D. K. Bhat, *Mater. Adv.*, 2022, 5941–5946.

7 U. S. Shenoy, K. D. Goutham and D. K. Bhat, *J. Alloys Compd.*, 2022, **905**, 164146.

8 D. K. Bhat and U. S. Shenoy, *J. Alloys Compd.*, 2020, **834**, 155181.

9 U. S. Shenoy and D. K. Bhat, *Energy Adv.*, 2022, **1**, 9–14.

10 D. K. Bhat and U. S. Shenoy, *J. Alloys Compd.*, 2020, **843**, 155989.

11 U. S. Shenoy and D. K. Bhat, *ACS Sustainable Chem. Eng.*, 2021, **9**, 13033–13038.

12 S. Shenoy and D. K. Bhat, *J. Phys. Chem. C*, 2017, **121**, 20696–20703.

13 H. J. Goldsmid, *J. Electron. Mater.*, 2012, **41**, 2126–2129.

14 A. T. Duong, V. Q. Nguyen, G. Duvjir, V. T. Duong, S. Kwon, J. Y. Song, J. K. Lee, J. E. Lee, S. Park, T. Min, J. Lee, J. Kim and S. Cho, *Nat. Commun.*, 2016, **7**, 1–6.

15 P. Qiu, X. Shi and L. Chen, *Energy Storage Mater.*, 2016, **3**, 85–97.

16 K. Zhao, P. Qiu, X. Shi and L. Chen, *Adv. Funct. Mater.*, 2020, **30**, 1–19.

17 K. Nishikawa, Y. Takeda and T. Motohiro, *Appl. Phys. Lett.*, 2013, **102**, 2012–2015.

18 S. Q. Bai, I. H. K. Wong, N. Zhang, K. Lin Ke, M. Lin, D. J. Young and T. S. A. Hor, *Dalton Trans.*, 2018, **47**, 16292–16298.

19 S. Q. Bai, I. H. K. Wong, M. Lin, D. J. Young and T. S. A. Hor, *Dalton Trans.*, 2018, **47**, 5564–5569.

20 Y. Bin Zhu, B. P. Zhang and Y. Liu, *Phys. Chem. Chem. Phys.*, 2017, **19**, 27664–27669.

21 K. Tyagi, B. Gahtori, S. Bathula, S. Auluck and A. Dhar, *Appl. Phys. Lett.*, 2014, **105**, 16–21.

22 T. Hu, Y. Yan, S. Wang, X. Su, W. Liu, G. Tan, P. Poudeu-Poudeu and X. Tang, *RSC Adv.*, 2019, **9**, 10508–10519.

23 Y. Jin, J. Hwang, S. Kim, J. Kim and S. J. Kim, *Nanoscale Adv.*, 2021, **3**, 3107–3113.

24 D. L. Shi, Z. M. Geng, L. Shi, Y. Li and K. H. Lam, *J. Mater. Chem. C*, 2020, **8**, 10221–10228.

25 J. Lei, Z. Ma, D. Zhang, Y. Chen, C. Wang, X. Yang, Z. Cheng and Y. Wang, *J. Mater. Chem. A*, 2019, **7**, 7006–7014.

26 L. Yang, Z. G. Chen, G. Han, M. Hong and J. Zou, *Acta Mater.*, 2016, **113**, 140–146.

27 A. A. Olvera, N. A. Moroz, P. Sahoo, P. Ren, T. P. Bailey, A. A. Page, C. Uher and P. F. P. Poudeu, *Energy Environ. Sci.*, 2017, **10**, 1668–1676.

28 B. Zhong, Y. Zhang, W. Li, Z. Chen, J. Cui, Y. Xie, Q. Hao and Q. He, *Appl. Phys. Lett.*, 2014, **105**, 1–4.

29 Z. Zhu, Y. Zhang, H. Song and X. J. Li, *Appl. Phys. A: Mater. Sci. Process.*, 2018, **124**, 747.

30 Q. Hu, Z. Zhu, Y. Zhang, X. J. Li, H. Song and Y. Zhang, *J. Mater. Chem. A*, 2018, **6**, 23417–23424.

31 S. Butt, W. Xu, M. U. Farooq, G. K. Ren, Q. Zhang, Y. Zhu, S. U. Khan, L. Liu, M. Yu, F. Mohmed, Y. Lin and C. W. Nan, *ACS Appl. Mater. Interfaces*, 2016, **8**, 15196–15204.

32 L. Yang, Z. G. Chen, G. Han, M. Hong, L. Huang and J. Zou, *J. Mater. Chem. A*, 2016, **4**, 9213–9219.

33 K. Zhao, M. Guan, P. Qiu, A. B. Blichfeld, E. Eikeland, C. Zhu, D. Ren, F. Xu, B. B. Iversen, X. Shi and L. Chen, *J. Mater. Chem. A*, 2018, **6**, 6977–6986.

34 F. H. Lin and C. J. Liu, *ChemSusChem*, 2021, **14**, 1316–1323.

35 H. Liu, X. Shi, M. Kirkham, H. Wang, Q. Li, C. Uher, W. Zhang and L. Chen, *Mater. Lett.*, 2013, **93**, 121–124.

36 A. L. N. Stevels and F. Jellinek, *Recl. Trav. Chim. Pays-Bas*, 1971, **90**, 273–283.

37 S. Ballikaya, H. Chi, J. R. Salvador and C. Uher, *J. Mater. Chem. A*, 2013, **1**, 12478.

38 Y. Qin, L. Yang, J. Wei, S. Yang, M. Zhang, X. Wang and F. Yang, *Materials*, 2020, **13**, 5704.

39 L. Zhao, X. Wang, F. F. Yun, J. Wang, Z. Cheng, S. Dou, J. Wang and G. J. Snyder, *Adv. Electron. Mater.*, 2015, 1400015.

40 K. Zhao, C. Zhu, P. Qiu, A. B. Blichfeld, E. Eikeland, D. Ren, B. B. Iversen, F. Xu, X. Shi and L. Chen, *Nano Energy*, 2017, **42**, 43–50.